A Linear Inertial Response Emulation for Variable Speed Wind Turbines

Azizipanah-Abarghooee, Rasoul; Malekpour, Mostafa; Dragicevic, Tomislav; Blaabjerg, Frede; Terzija, Vladimir

Published in:
I E E E Transactions on Power Systems

DOI (link to publication from Publisher):
10.1109/TPWRS.2019.2939411

Publication date:
2020

Document Version
Accepted author manuscript, peer reviewed version

This article has been accepted for publication in a future issue of this journal, but has not been fully edited. Content may change prior to final publication. Citation information: DOI 10.1109/TPWRS.2019.2939411, IEEE Transactions on Power Systems

A Linear Inertial Response Emulation for Variable Speed Wind Turbines

Rasoul Azizipanah-Abarghooee, *Senior Member, IEEE*, Mostafa Malekpour, *Student Member, IEEE*, Tomislav Dragičević, *Senior Member, IEEE*, Frede Blaabjerg, *Fellow, IEEE*, and Vladimir Terzija, *Fellow, IEEE*

***Abstract*—A torque limit-based (TLB) method was proposed in literature in order to emulate inertial response of variable speed wind turbines (VSWTs). In this paper, this conventional TLB scheme is firstly modified by considering a finite ramp rate for inertial power of the VSWT. It is exposed that the maximum values of the VSWT's inertial power and kinetic energy released by its rotor have a non-linear relationship with its operation point. Then, a linear TLB scheme is proposed to make the inertia emulation more flexible by customizing its key parameters based on the VSWT's operating point. Accordingly, the released kinetic energy and power ramp rate can be selected in proportion of the VSWT's power, rotor speed and/or its reserved kinetic energy. The derived scheme offers a significant reduction of the mechanical tensions on the turbine compared to the conventional one. In addition, when the parameters of the proposed strategy is designed according to the VSWT's power, the inertial response of the corresponding wind farm can be exactly estimated only by deploying its total generation, regardless of its wind turbines' installed capacities and operating points. Furthermore, a new approach is projected to estimate the VSWT's inertial response during the deceleration period using an analytical closed-form function. This facilitates large scale system studies. Finally, the efficiency of derived linear inertia emulation is evaluated through a typical grid with various levels of the wind power penetration.**

***Index Terms*—Frequency support, inertial response estimation, linear inertia emulation, torque limit, variable speed wind turbines.**

I. Introduction

INERTIAL response provided by synchronous generators (SGs) plays an important role in the power systems' frequency regulation mechanism. In contrast, this fundamentally crucial feature of power systems would change dramatically with the increase of the penetration level of converter-based generations such as variable speed wind turbines (VSWT) [1], [2]. Inertial response of the VSWTs is filtered by power converters in conventional control strategies aimed to achieve maximum power point tracking (MPPT). To overcome this problem, researchers have proposed several solutions to add an auxiliary control loop to wind turbine's (WT's) controllers to emulate the inertial response of the SGs.

A complementary control loop to emulate inertial response for the VSWTs is presented in [3]. This inertia emulator (IE) is designed based on the swing equation to add a frequency-dependent torque component to the reference torque obtained from the MPPT algorithm. The impact of rotor current controller's bandwidth in a doubly fed induction generator (DFIG) on its electric power variations following an abrupt frequency excursion is investigated in [4]. It is deduced that the lower the value of this bandwidth is, the higher DFIG's inertial response is. An IE consisting of a loop with the rate-of-change-of-frequency (RoCoF) and frequency deviation as its input are derived in [3] and [5], respectively. The DFIG is able to inject more inertial response to the network using the later one. This certainly reduces the WT's speed, which in turn leads to more power drawn from the network by WT in order to recover its speed. A DFIG provides inertial response even without IE if its converter controls the stator power, however, the WT's speed will keep decreasing towards unstable operation if the frequency does not recover [6]. Additionally, the WT's rotor speed recovery may be problematic while the converter adjusts electrical power and the gain and time constant of the IE are not properly tuned. In this regard, an adaptive-gain inertial control is proposed in [7] to ensure stable operation of WTs. To increase the kinetic energy extraction from the WT rotor immediately following an event and simultaneously reduce the impact of the inertia emulator on the WT rotor speed, the time-varying and speed-varying inertia gains are used in [8] and [9]-[10], respectively.

An improper common practice in designing inertia emulators was to neglect the maximum torque tolerated by the generator. In this context, a torque limit-based (TLB) scheme is derived in [11] to maximize the inertial response taking into account the maximum torque limit. However, it reduces the WT's inertial power rapidly, which causes a late but substantial frequency nadir [12]. To make this less severe, it was suggested that the inertial power should be instantly increased to a fixed value upon detecting an event and then it maintains this value for a preset time [12]. The main advantage of this scheme is that the incremental power varies with both WT's rotor speed and wind penetration level [12]. On the other hand, there was no algorithm to derive the value of this preset time and it was determined through simulations.

To reduce the adverse effect of WT's rotor speed recovery on the network frequency, the WTs of a wind farm should be divided into several groups and their contributions in the inertial power will be determined consecutively [13]. An inertial response proportional to the frequency variation with time variant controlling gain is proposed in [14] in order to considerably enhance the WT's speed recovery procedure in comparison with [13]. Another WT's speed recovery strategy is projected in [15] to smoothly perform the transition from inertial power to speed recovery modes. It is also suggested that the rate of WT's power reduction should be restricted during transition from inertial response to the speed recovery in order to reduce the WT's mechanical tensions [16].

The dynamic behavior of the WTs equipped with IE is highly dependent on the pre-event operating point. It is shown that the inertial energy reaches its maximum value at a wind speed lower than the nominal one [16]. In [17], the emulated

Manuscript received December 29, 2018; revised March 11, 2019 and June 29, 2019; accepted August 11, 2019. This work was supported by the Enhanced Frequency Control Capability (EFCC) project that is funded under the GB's Network Innovation Competition. Paper no. TPWRS-01958-2018. *(Corresponding author: Rasoul Azizipanah-Abarghooee.)*

R. Azizipanah-Abarghooee and V. Terzija are with the Department of Electrical and Electronic Engineering, The University of Manchester, Manchester M13 9PL, U.K. (e-mail: rasoul.azizipanah@manchester.ac.uk; vladimir.terzija@manchester.ac.uk)

M. Malekpour is with the department of electrical engineering, University of Isfahan, Isfahan, Iran (e-mails: M.malekpour@eng.ui.ac.ir)

T. Dragicevic and F. Blaabjerg are with the Department of Energy Technology, Aalborg University, 9220 Aalborg East, Denmark (e-mail: tdr@et.aau.dk; fbl@et.aau.dk)

This article has been accepted for publication in a future issue of this journal, but has not been fully edited. Content may change prior to final publication. Citation information: DOI 10.1109/TPWRS.2019.2939411, IEEE Transactions on Power Systems

inertial power is analytically calculated for a VSWT based on the allowed minimum WT's shaft speed and the desirable time to inject the inertial power to the grid. Furthermore, the required amount of WT's speed increment to operate at a sub-optimal point is derived by approximating the WT's power coefficient in [18] considering the permissible minimum value of the grid frequency. The dynamics of the WT type 4 is studied in [19] during the inertial power injection to the grid. The derived IEs have this ability to operate in two conditions of constant set-point and variable set-point. The inertial power depends to the grid frequency deviation and wind speed variation. A proportional-integral controller with the input of WT's rotor speed deviation from its reference value can determine the electric power reference during the WT's rotor speed recovery [20]. This allows adjusting the amount of power reduction during speed recovery and thus its negative effect on the grid will be considerably mitigated.

In this paper, the conventional TLB inertia emulation scheme presented in [11] is firstly modified considering a finite ramp rate for the WT's inertial power. Then, its characteristics are analytically derived for different operating points of the WT. It is deduced that the derived characteristics have non-linear relationship with the WT's operating point. In particular, the kinetic energy released by the WT rotor maximizes below its nominal speed. In order to make the TLB scheme more flexible, it is modified by customizing its key parameters. The main goal of this customization is to make a linear relation between characteristics of the proposed TLB method and the WT operating point. In the proposed scheme:

1) The amount of released kinetic energy and inertial power ramp rate can be selected in proportion with the WT's power, rotor speed and/or reserved rotor's kinetic energy.
2) The starting time of the WT's rotor speed recovery is identical for all operating points of the wind turbine.
3) Mechanical parts of the turbine experience less stress, particularly at low rotor speeds in comparison with the conventional TLB scheme.
4) The WT's inertial power during the deceleration period can be estimated by a closed-from analytical function to facilitate the power systems' frequency assessment.
5) The inertial response of a wind farm can be exactly estimated only by using its total generation, regardless of wind turbines' installed capacities and operating points.

This paper is organized as: Section II introduces concisely the WT's aerodynamics. The conventional TLB IE is modified and examined in Section III. The proposed linear TLB scheme is described in Section IV. The simulation results are provided in section V. Finally, Section VI concludes the paper.

II. Wind Turbine Aerodynamics

The mechanical power generated by a wind turbine (P_m) is:

$$P_m = 0.5 C_P \rho \pi R^2 V^3 \quad (1)$$

where ρ, R and V are air density, rotor radius and wind speed, respectively. In VSWTs, C_P is WT's power coefficient which is a function of the blade pitch angle θ and tip speed ratio λ. It can be defined as follows [21]:

$$\lambda = R\omega\, V^{-1} \quad (2)$$

where, ω denotes the mechanical angular speed of the rotor. The C_P can be traditionally calculated as follows [22]:

$$C_P = c_1\left(\frac{c_2}{\lambda_i} - c_3\theta - c_4\theta^{c_5} - c_6\right)e^{-\frac{c_7}{\lambda_i}}, \quad \frac{1}{\lambda_i} = \frac{1}{c_8\theta + \lambda} - \frac{c_9}{\theta^3 + 1} \quad (3)$$

The maximum P_m can be achieved at the optimum tip speed ratio $\lambda_{C_{Pmax}}$ where C_P has its maximum value C_{Pmax}. For the WT operation below rated wind speed, the pitch angle θ is equal to zero [21]. Then, taking the derivative of C_P in (3) with respect to λ and equalize it to zero yields:

$$\lambda_{C_{P_{max}}} = c_2 c_7 \left(c_2 + c_6 c_7 + c_2 c_7 c_9\right)^{-1} \quad (4)$$

In VSWTs, $\lambda_{C_{Pmax}}$ is maintained and power captured by the WT is maximized known as MPPT control [11]. In this study, a generic form of (1) is derived where the parameter k_1 is:

$$k_1 = \lambda_{C_{P_{max}}} V_{nom} \omega_{Vnom}^{-1} \quad (5)$$

where, V_{nom} and ω_{Vnom} are the nominal wind speed and the WT speed at V_{nom}, respectively. Thus, (2) is expressed as:

$$\lambda = K_1 \omega\, V^{-1} \quad (6)$$

In the other hand, the parameter k_2 is defined by:

$$k_2 = P_{mVnom} C_{Pmax}^{-1} V_{nom}^{-3} \quad (7)$$

where, P_{mVnom} denotes the wind turbine power at V_{nom}. Therefore, (1) may be rewritten as:

$$P_m = k_2 C_P V^3 = k_2 C_P \left(k_1 \omega\right)^3 \lambda^{-3} \quad (8)$$

The optimum turbine power P_{opt} is obtained by substituting the optimum tip speed ratio into the above equation as:

$$P_{opt} = k_2 C_{Pmax} \left(k_1 \lambda_{C_{Pmax}}^{-1}\right)^3 \omega^3 = k_{opt}\omega^3 \quad (9)$$

$$k_{opt} = P_{mVnom}\omega_{Vnom}^{-3} \quad (10)$$

III. The Conventional Torque Limit-Based Approach

The main aim of the conventional TLB IE scheme is to extract maximum kinetic energy from WT's rotor. Note, the WT can generate more electrical power than its mechanical one through its rotor speed reduction. This power comes from the stored kinetic energy in its rotor. The characteristics of this method are illustrated by the ADC trajectories in Fig. 1. Here, the WT's electrical power P_e is governed by [11]:

$$P_e = P_{min} + k_e\left(\omega - \omega_{min}\right) \quad (11)$$

$$k_e\langle\omega_0\rangle = \left(P_{max}\langle\omega_0\rangle - P_{min}\right)\left(\omega_0 - \omega_{min}\right)^{-1} \quad (12)$$

$$P_{max}\langle\omega_0\rangle = T_{max}\omega_0, \quad P_{min} = k_{opt}\omega_{min}^3 \quad (13)$$

with ω_{min} and T_{max} as the permissible minimum rotor speed and the maximum electrical torque, respectively. ω_0 is the pre-event rotor speed. In fact, k_e is the slope of the DC line in Fig. 1.a. With an infinite ramp rate, it can be observed that the electric torque is only maximal at t_0, i.e. the frequency event

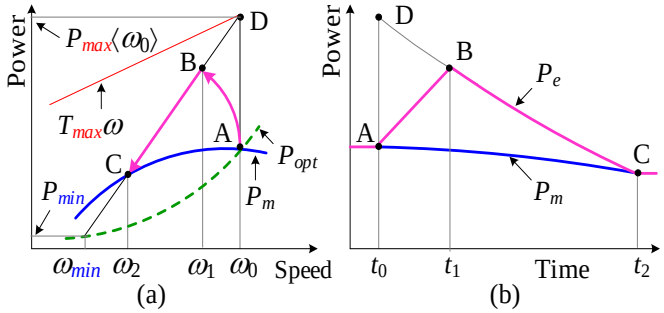

Fig. 1. Operational characteristics of the TLB inertia emulation schemes.

This article has been accepted for publication in a future issue of this journal, but has not been fully edited. Content may change prior to final publication. Citation information: DOI 10.1109/TPWRS.2019.2939411, IEEE Transactions on Power Systems

instant, and it decreases over the time. With the assumption of ω_{min} equal to zero, the torque remains maximum for all intervals ranged from t_0 to t_2. It will cause the kinetic energy to be injected into the network in the shortest possible time. However, it will be difficult to establish the rotor speed stability in this case, and sudden electric power decrement leads to a second frequency dip [11]. Taking into account a finite power ramp rate, ABC trajectory represents the modified conventional TLB scheme. The quantities of this modified scheme are derived hereinafter. It is assumed that the pre-event WT speed must be greater than ω_{0min} in order to activate the inertia emulator. Thus, it can be exposed as:

$$\omega_{0_{min}} = \omega_{min} + \Delta\omega_{th} \tag{14}$$

where, $\Delta\omega_{th}$ is the required threshold for the WT's speed. By defining a power ramp rate R_P, (11) can be rewritten as:

$$P_e = min\left(P_{min} + k_e\left(\omega - \omega_{min}\right),\ P_{e0} + R_P t\right) \tag{15}$$

where, P_{e0} denotes the pre-event optimal WT's electrical power. For a zero pitch angle, the mechanical power $P_m\langle\omega\rangle$ at an arbitrary speed ω for the pre-event speed ω_0 should be estimated by C_P approximation using Taylor's series. This derives the coefficients a, b and c as follows:

$$P_m\langle\omega\rangle \approx a(\omega-\omega_0)^2 + b(\omega-\omega_0) + c \tag{16}$$

where

$$a = c_1 a_3 k_1^2 k_2 \omega_0 \left(k_{opt} k_2^{-1} C_{P\,max}^{-1}\right)^{1/3}$$
$$\left(c_2 a_2 \lambda_{C_{P\,max}}^{-1} + \left(c_7 a_2 \lambda_{C_{P\,max}}^{-1} - 0.5 c_7^2 a_2^2\right)\left(c_6 + a_1 c_2\right) - c_2 c_7 a_2^2\right)$$
$$b = -c_1 a_3 k_1 k_2 \omega_0^2 \left(k_{opt} k_2^{-1} C_{P\,max}^{-1}\right)^{2/3}\left(c_2 a_2 + c_7 a_2\left(c_6 + c_2 a_1\right)\right) \tag{17}$$
$$c = -c_1 a_3 k_{opt} C_{P\,max}^{-1} \omega_0^3 \left(c_6 + c_2 a_1\right),\ a_3 = exp\left(c_7 a_1\right)$$
$$a_1 = \lambda_{C_{P\,max}}^{-1}\left(\lambda_{C_{P\,max}} c_9 - 1\right),\ \ a_2 = \lambda_{C_{P\,max}}^{-1}\left(c_9 - a_1\right)$$

Now, the WT's swing equation during time interval (t_0, t_1) can be described as follows:

$$P_m\langle\omega\rangle - \left(P_{e0} + R_P t\right) = M\,\omega\langle t\rangle \frac{d\omega\langle t\rangle}{dt} \tag{18}$$

where M is the combined mechanical time constant of the WT's and generator's shafts. Here, t_0 is considered to be the time origin. Although there is no straightforward solution for obtaining $\omega\langle t\rangle$ from (18), it can be approximated using Taylor series. To this end, taking time derivative of (18) yields:

$$\frac{d^2\omega\langle t\rangle}{dt^2} = \frac{1}{M\,\omega\langle t\rangle}\left(\frac{d}{dt}P_m\langle\omega\rangle - R_P - M\left(\frac{d\omega\langle t\rangle}{dt}\right)^2\right) \tag{19}$$

By calculating the time-domain derivative of $P_m\langle\omega\rangle$ and its replacement with (19), it gives:

$$\frac{d^2\omega}{dt^2} = \frac{1}{M\,\omega}\left(\left(2a(\omega-\omega_0)+b\right)\frac{d\omega}{dt} - R_P - M\left(\frac{d\omega}{dt}\right)^2\right) \tag{20}$$

Finally, (21) can be provided from (18) and (20):

$$\frac{d\omega\langle t\rangle}{dt}\langle t=0\rangle = 0,\quad \frac{d^2\omega\langle t\rangle}{dt^2}\langle t=0\rangle = -\frac{R_P}{M\,\omega_0} \tag{21}$$

Therefore, $\omega\langle t\rangle$ can be approximated as follows:

$$\omega\langle t\rangle \approx \omega_0 - R_P(2M\omega_0)^{-1}t^2 \tag{22}$$

Considering R_P as ramp rate, point B in Fig. 1 shows the maximum inertial power. The time to reach to this point is indicated by t_1. This parameter can be calculated by equating two arguments located in parenthesis of (15) as follows:

$$P_{e0} + R_P t_1\langle\omega_0\rangle = P_{min} + k_e\left(\omega\langle t = t_1\rangle - \omega_{min}\right) \tag{23}$$

Substituting (22) into (23) and solving the result for t_1 yields:

$$t_1\langle\omega_0\rangle = M\omega_0 k_e^{-1}\left(-1 + \sqrt{1 + 2k_e R_P^{-1} M^{-1}\left(T_{max} - k_{opt}\omega_0^2\right)}\right) \tag{24}$$

Hence, the WT's rotor speed ω_1 is given by:

$$\omega_1\langle\omega_0\rangle = \omega_0 - R_P\left(2M\omega_0\right)^{-1} t_1^2 \tag{25}$$

After instant t_1, the amount of inertial power is determined by the BC line. The electrical power is identical with the WT's mechanical power at point C. Accordingly, t_2 can be also calculated as follows:

$$t_2\langle\omega_0\rangle = t_1 + M\int_{\omega_1}^{\omega_2} \frac{\omega\, d\omega}{P_m\langle\omega\rangle - P_{min} - k_e(\omega - \omega_{min})} \tag{26}$$

The parameter t_2 can be calculated using indefinite integral of right-hand side of the above equation as follows:

$$\int \frac{\omega\, d\omega}{P_m\langle\omega\rangle - P_{min} - k_e(\omega-\omega_{min})} =$$
$$\frac{1}{2a} ln\left(a\left(\omega-\omega_0\right)^2 + b'\left(\omega-\omega_0\right) + c'\right) \tag{27}$$
$$+ \frac{2a\omega_0 - b'}{a\sqrt{4ac' - b'^2}}\, tan^{-1}\left(\frac{2a\left(\omega-\omega_0\right)+b'}{a\sqrt{4ac'-b'^2}}\right)$$

where,

$$b' = b - k_e,\quad c' = c - P_{min} + k_e\omega_{min} \tag{28}$$

However, the speed ω_2 must be determined before calculating t_2. To do this, ω should be replaced with ω_2 in (11) and (16) and it can be achieved as follows:

$$\omega_2\langle\omega_0\rangle = \omega_0 - \left(b' + \sqrt{b'^2 - 4ac''}\right)\left(2a\right)^{-1} \tag{29}$$

$$c'' = c - P_{min} - k_e(\omega_0 - \omega_{min}) \tag{30}$$

After which, t_2 can also be obtained from (26), however, it will be an infinite value. The mathematical reason behind this fact is that the term inside the integral of (26) tends to infinity by moving from point B to C. The physical reason is that the deceleration torque tends to be zero by moving towards point C and as such the speed will never reduce to ω_2. Therefore, t_2 is calculated for a value more than ω_2 denoted by ω_2'. It represents the rotor speed in which the k_{ke} fraction of the stored kinetic energy in the rotor is released by speed reduction from ω_0 to ω_2. k_{ke} can be formulated as follows:

$$k_{ke} = (\omega_0^2 - \omega_2'^2)(\omega_0^2 - \omega_2^2)^{-1} \tag{31}$$

Consequently, solving the above equation for ω_2' yields:

$$\omega_2'\langle\omega_0\rangle = \sqrt{\omega_0^2 - k_{ke}\left(\omega_0^2 - \omega_2^2\right)} \tag{32}$$

The released kinetic energy KE_{rel}, through the WT's rotor speed reduction from ω_0 to ω_2' is:

$$KE_{rel} = 0.5M(\omega_0^2 - \omega_2'^2) \tag{33}$$

Fig. 2 portrays all the quantities related to the modified conventional TLB scheme for a wind turbine with parameters listed in Table I. The horizontal axes in the upper and lower sides represent the pre-event WT speed and power quantities, respectively. Note that top ticks are shown in non-linear scale since the power's ticks have linear scale. Here, the minimum speed required to activate IE is assumed to be 0.65 *p.u.* The R_P is assumed to be 0.05 *p.u.*/s. It can be observed that the maximum amount of t_1 and thus that of the inertial power occur at an operating point lower than the nominal one. This is also applicable with the released kinetic energy KE_{rel}, while its

This article has been accepted for publication in a future issue of this journal, but has not been fully edited. Content may change prior to final publication. Citation information: DOI 10.1109/TPWRS.2019.2939411, IEEE Transactions on Power Systems

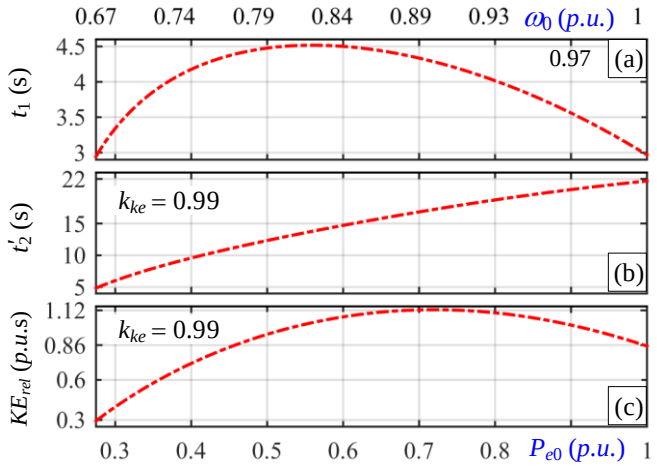

Fig. 2. The characteristics of the modified conventional TLB scheme.

TABLE I
PARAMETERS OF THE STUDIED WIND TURBINE [23]

V_{nom}	11.8 m/s	ω_{Vnom}	1 $p.u.$	M	10.5 s	$\Delta\omega_{th}$	0.05 $p.u.$
T_{max}	1.2 $p.u.$	P_{mVnom}	1 $p.u.$	ω_{min}	0.6 $p.u.$	R_P	0.05 $p.u./s$
$c_{1-9} = [0.279, 118, -0.5, 0.922, 1.12, 3.33, 15.6, 0.102, 0.017]$							

corresponding maximum point differs from that associated one with t_1. It is to be noted that the unit of the vertical axis in Fig. 2.c is per-unit per seconds. It can be seen from Fig. 2.b that the time interval of the inertial power injection varies from 5 to 22 seconds. The most important characteristic of the traditional TLB quantities shown in Fig. 2 is their non-linearity with the WT operating point.

IV. The Proposed Torque Limit-Based Approach

In this section, the traditional TLB method is modified in such a way as to make a linear relationship between the quantities shown in Fig. 2 and the WT's operating point. In the proposed method, the following relationship holds between released kinetic energy for an arbitrary pre-event speed ω_0 and that of the minimum speed to activate IE i.e. ω_{0min}:

$$\frac{KE_{rel}\langle\omega=\omega_0\rangle}{KE_{rel}\langle\omega=\omega_{0min}\rangle}=\frac{0.5M\left(\omega_0^2-\omega_2'^2\right)}{0.5M\left(\omega_{0min}^2-\omega_{2min}'^2\right)}=\left(\frac{\omega_0}{\omega_{0min}}\right)^N \quad (34)$$

where, N can be an integer value from 1 to 3. While it is 1, KE_{rel} for two speed values is proportional to the ratio of those two speeds. In the case of $N = 2$, KE_{rel} is proportional to the KE value corresponding to these two speeds. Finally, KE_{rel} for the two speeds is proportional to the WT's power at those two speeds in case of $N = 3$. Then, solving (34) for ω_2' yields:

$$\omega_2'\langle\omega_0\rangle=\sqrt{\omega_0^2-\left(\omega_0\left(\omega_{0min}\right)^{-1}\right)^N\left(\omega_{0min}^2-\omega_{2min}'^2\right)} \quad (35)$$

On the other hand, the power ramp-up rate for an arbitrary speed ω_0 is calculated in a similar way with KE_{rel} but based on the ramp rate of the maximum speed R_{Pmax} as follows:

$$R_P\langle\omega_0\rangle=(\omega_0(\omega_{0max})^{-1})^N R_{Pmax} \quad (36)$$

Then, the slope of the BC segment shown in Fig. 1.a can be calculated for the maximum speed k_{emax} as follows:

$$k_{emax}=\left(T_{max}\omega_{0max}-P_m\langle\omega_0=\omega_{2max}'\rangle\right)\left(\omega_{0max}-\omega_{2max}'\right)^{-1} \quad (37)$$

Therefore, by calculating (36) and (37) for the maximum speed and then substituting the results into (24), the critical time t_1 for the maximum speed will be determined. After defining the vital parameters of the ABC path for the maximum speed ω_{0max}, the parameters associated with speeds less than ω_{0max} is calculated hereinafter. As a feature of the proposed method, it is assumed that the inertial power value for all speeds less than ω_{0max} reaches its maximum point after the same time with that of ω_{0max}. Thus, it gives:

$$t_1\langle\omega=\omega_0\rangle=t_1\langle\omega=\omega_{0max}\rangle \quad (38)$$

If the left-hand side of (38) is substituted by (24) and solving the result for the maximum torque of the speed ω_0, i.e., $T_{max}\langle\omega_0\rangle$ it yields:

$$T_{max}\langle\omega_0\rangle=\frac{k_{opt}d\omega_0^4\left(\omega_2'-\omega_0\right)+t_1\omega_0\left(\omega_2'+\omega_0\right)+0.5t_1^2M^{-1}P_m\langle\omega=\omega_2'\rangle}{d\omega_0^2\left(\omega_2'-\omega_0\right)+0.5M^{-1}t_1^2\omega_0} \quad (39)$$

$$d=\left(R_P\langle\omega_0\rangle\right)^{-1} \quad (40)$$

By determining the maximum permissible torque for speed ω_0, the slope of BC line can be obtained for this velocity as:

$$k_e\langle\omega_0\rangle=\left(T_{max}\langle\omega_0\rangle\ \omega_0-P_m\langle\omega=\omega_2'\rangle\right)\left(\omega_0-\omega_2'\right)^{-1} \quad (41)$$

Thus, the parameters of the ABC path are determined for all speeds ranging from ω_{0min} to ω_{0max}.

In this context, it's quite fruitful to provide further explanations. The traditional TLB method's path can be characterized by identification of three points A, D, and C as shown in Fig. 1. These points can be specified by determining the maximum allowable WT's electrical torque and its minimum speed limit. In this scheme, both limits are presumed to be identical for all pre-event WT speeds. Eventually, point B can be also specified by choosing a power ramp rate R_P for all operating points. In contrast, in the proposed TLB method, the objective is to set the permissible values of maximum torque $T_{max}\langle\omega_0\rangle$ and speed ω_2' for discrepant values of ω_0 in such a way that (34) is applicable for the released kinetic energy at two different speeds. A flowchart illustrating the proposed TLB method is provided in Fig. 3. The first main step calculates t_1 for the maximum speed. In the second stage, the maximum torque $T_{max}\langle\omega_0\rangle$ for pre-event speed ω_0 is determined so that (38) will be satisfied. Finally, the slope of BC line shown in Fig. 1.a, i.e., $k_e\langle\omega_0\rangle$, is calculated to hold the relationship mentioned in (34).

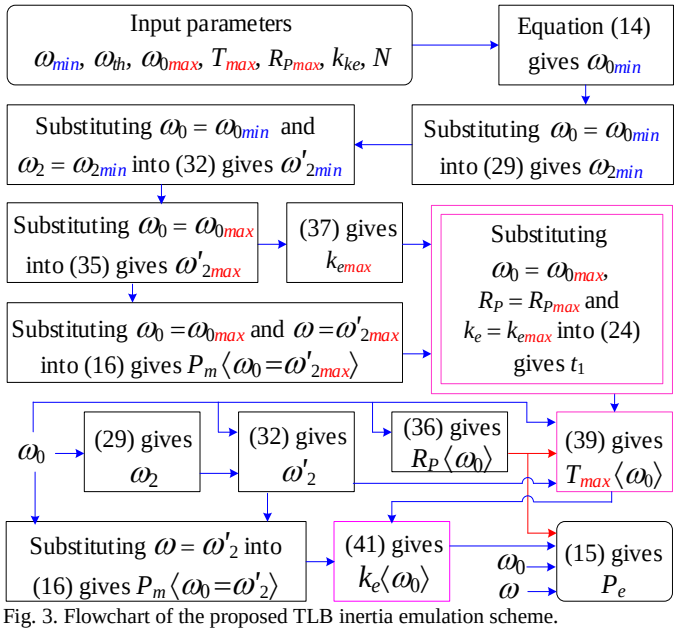

Fig. 3. Flowchart of the proposed TLB inertia emulation scheme.

This article has been accepted for publication in a future issue of this journal, but has not been fully edited. Content may change prior to final publication. Citation information: DOI 10.1109/TPWRS.2019.2939411, IEEE Transactions on Power Systems

The characteristics of the proposed method are plotted in Figs. 4 and 5 along with the traditional ones. It is clear-cut from Fig. 4.a that the released kinetic energy in the proposed method is less than the traditional one (with the exception of $P_{e0} > 0.92$ for $N = 3$). However, in the proposed method, this quantity corresponds to N equal to 1, 2 and 3 is proportional to the speed, speed square and power of the WT, respectively. On the other hand, the power ramp rate $R_P\langle\omega_0\rangle$ decreases with WT power decrement in the proposed approach, while it has a fixed value for the conventional method. Moreover, the maximum permissible torque obtained from (39) reduces with decreasing the power. In Fig. 4.d, both schemes are compared in terms of slope of BC line. In the conventional method, this slope increases dramatically with the decrease of the WT power, while it decreases slightly in the proposed method.

The methods are also compared in Fig. 5 in terms of electrical power and torque. As can be seen from Fig. 5.a, the maximum amount of electrical power increment following the incident (at point B in Fig. 1) in the proposed method is less than the traditional one. However, it has a linear behavior with the WT's operating point. The maximum electrical torque

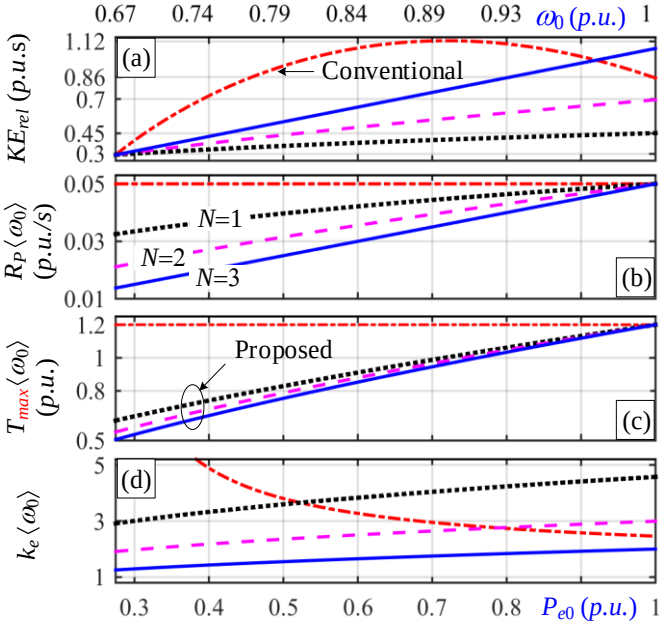

Fig. 4. The characteristics of the proposed TLB scheme.

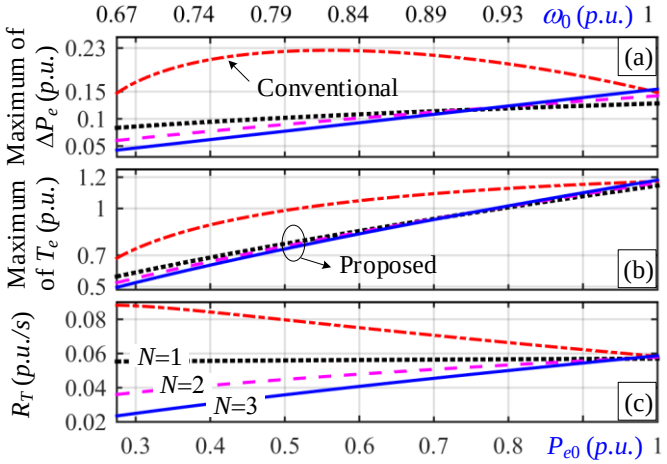

Fig. 5. (a) The maximum electrical power deviation, (b) the maximum electrical torque and (c) the averaged torque ramp rate of the wind turbine.

corresponding to the powers in Fig. 5.a is shown in Fig. 5.b. The difference between this quantity and its permissible limit $T_{max}\langle\omega_0\rangle$, portrayed in Fig. 4.c, increases with the WT power reduction in the traditional approach. However, this discrepancy is minor for all the WT operating points in the modified method. Finally, the methods are compared from the viewpoint of average rate of torque increment R_T from the event instant to t_1 as shown in Fig. 5.c. This is obtained as:

$$R_T = \left(\left(P_{e0} + \Delta P_{e\,max}\right)\omega_1^{-1} - P_{e0}\omega_0^{-1}\right)t_1^{-1} \tag{42}$$

By comparing the proposed method with the traditional one in terms of R_T, it is exposed that albeit traditional method produces more inertial power in lower power values, it is accompanied with a significant increment of stress on WT's shaft. On the other hand, the lower torque increment rate is one of the major benefits of the proposed method along with its linear characteristics. In particular, the value of R_T is decreased in the proposed scheme with increasing N.

The inertial responses of the WT provided by both TLB schemes are shown in Fig. 6. Here, the pre-event speed ω_0 ranges from 0.65 to 1 *p.u.* with 0.05 *p.u.* incremental step. It can be seen that in the conventional method, the shape of the electrical power is highly dependent on the WT's operating point, while this is not the case with the proposed method. In this method, regardless of the pre-event WT operating point, the inertial power reaches its maximum limit after 3 seconds.

For analysis purpose, it is convenient to model available WT's inertial response by a closed-form function to assess their contribution to the short-term frequency regulation at the power system-level [24], [25]. In this context, a new approach is proposed to analytically estimate the inertial response of the WTs which are controlled by the proposed TLB scheme. It can be deduced from Fig. 6.b that the electrical power is reduced exponentially after t_1. To obtain the time constant of this exponential function, the linear relationship between velocity and electrical power in (14) is taken into account. The WT speed can be estimated as follows:

$$\hat{\omega}\langle t\rangle = \omega_2' + \left(\omega_1 - \omega_2'\right)exp\left(-(t-t_1)\tau^{-1}\right) \quad \text{for} \quad t > t_1 \tag{43}$$

On the other hand, the electrical and mechanical powers between points B and C can be expressed as follows:

$$P_e = P_m\langle\omega = \omega_2'\rangle + k_e\left(\omega - \omega_2'\right) \tag{44}$$

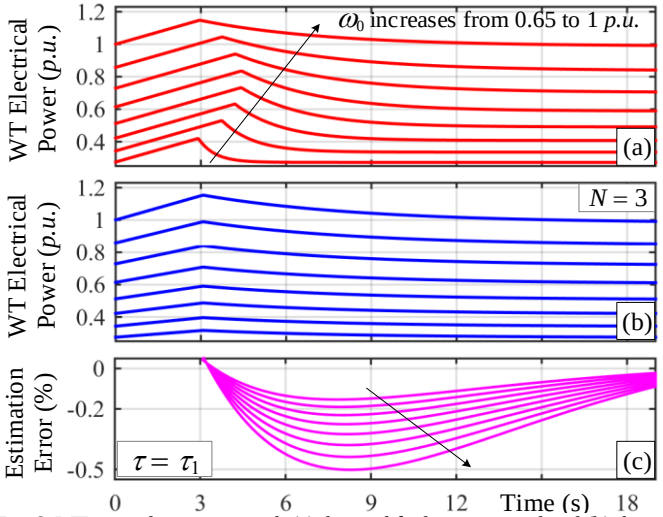

Fig. 6. WT inertial responses with (a) the modified conventional and (b) the proposed TLB schemes; (c) the inertial response estimation error.

This article has been accepted for publication in a future issue of this journal, but has not been fully edited. Content may change prior to final publication. Citation information: DOI 10.1109/TPWRS.2019.2939411, IEEE Transactions on Power Systems

$$P_m \approx P_m\langle\omega=\omega_2'\rangle + k_m\left(\omega-\omega_2'\right) \quad (45)$$

$$k_m = \left(P_m\langle\omega=\omega_1\rangle - P_m\langle\omega=\omega_2'\rangle\right)\left(\omega_1-\omega_2'\right)^{-1} \quad (46)$$

In the abovementioned equations, the mechanical power is approximated by a first-order polynomial. Next, substituting (43)-(46) into the equation (18) and rearranging yields:

$$\tau = M\left(k_e - k_m\right)^{-1}\omega\langle t\rangle \quad (47)$$

It is clear that the derived time constant τ has a time-variable nature. To solve this difficulty, two values are defined for τ ignoring k_m with respect to k_e as follows:

$$\tau_1 = k_e^{-1}M\omega_1, \quad \tau_2 = k_e^{-1}M\omega_2' \quad (48)$$

Finally, the electrical power can be estimated as follows:

$$\hat{P}_e\langle t\rangle = P_m\langle\omega=\omega_2'\rangle + k_e\left(\omega_1-\omega_2'\right)exp\left(-\left(t-t_1\right)\tau^{-1}\right),\ t>t_1 \quad (49)$$

The inertial power trends shown in Fig. 6.b are estimated using (49) and their estimation errors are illustrated in Fig. 6.c. These results indicate that (49) works well under τ_1.

To restore the WT's rotor speed, its electrical power is determined by (50) in order to establish a trade-off between the time needed for WT's rotor speed recovery and the power drawn from the power system as follows:

$$P_{rec} = 0.99P_m\langle\omega=\omega_2'\rangle + k_{rec}\left(\omega-\omega_2'\right)^2 \quad (50)$$

$$k_{rec} = \left(P_{e0} - 0.99P_m\langle\omega=\omega_2'\rangle\right)\left(\omega_0-\omega_2'\right)^{-2} \quad (51)$$

The characteristics associated with (50) are depicted in Fig. 7. This relationship is equation of the EA curve shown in Fig. 7.a. In order to reduce the shaft torque fluctuations, a down-rate limiter should be deployed to restrict the power decrement rate immediately following the speed recovery interval. In this case, the WT's electrical power is gradually reduced from C′ to E′. In this study, this rate is set to R_{Pmax}. The factor 0.99 is used in (50)-(51) to ensure positivity of acceleration torque.

V. Simulation Results

This section applies the TLB methods described in sections III and IV to evaluate their performance. The studied power system is firstly described. Then, the proposed strategy is compared against the modified conventional one through the time-domain simulations.

A. The System Description

The studied power system is implemented in DIgSILENT PowerFactory 2018, as shown in Fig. 8. The system's demand is simulated by a 1000 MW, 100 MVar general load (GL) element. Load damping constant is 2%/Hz [26]. The steam turbine (ST) unit supplies 5% of the system's demand. The gas turbine (GT) plant is selected as slack machine. A wind farm is integrated into the system through a transformer and a 50 km transmission line. A STATCOM is deployed for the sake of voltage support at the wind farm location. To measure the wind farm installed capacity, the k_{ic} is defined as follows:

$$k_{ic} = 100\left(P_{wf\,max}P_d^{-1}\right) \quad (52)$$

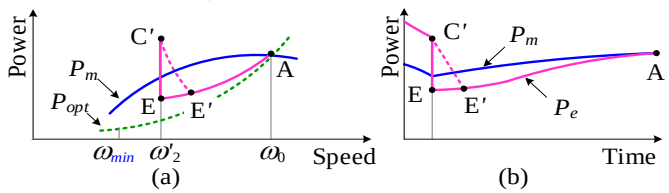

Fig. 7. Characteristics of the proposed WT speed recovery scheme.

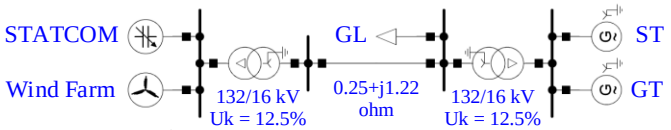

Fig. 8. Schematic of the studied power system in DIgSILENT PowerFactory.

where, P_{wfmax} and P_d represent the wind farm installed capacity and the system's demand, respectively. On the other hand, the following parameter k_{op} is employed to calculate the operating point of the wind farm as follows:

$$k_{op} = 100\left(P_{wf}P_{wf\,max}^{-1}\right) \quad (53)$$

where, P_{wf} denotes the farm active power. In fact, multiplying (52) by (53) gives the wind penetration level. The performance of the proposed TLB scheme is compared with that of the conventional one under four various case studies. The power flow results are illustrated in Table II for these scenarios. In this table, S, P and Q denote apparent, active and reactive powers, respectively. The installed capacity of the wind farm is 40% in the first case, while it is 80% of the system demand in the second one. In the first two case studies, it is assumed that the wind farm consists of 10 identical wind turbines which operate in a similar operating point. However, this is not the case for the third and fourth study cases, in which the wind farm's power P_{wf} is calculated as follows:

$$P_{wf} = \frac{\sum_{i=1}^{10}(0.25i)P_{wt,i}}{\sum_{i=1}^{10}(0.25i)} \quad (54)$$

where $P_{wt,i}$ is active power of the i^{th} wind turbine. Detailed data of the wind turbines are provided in Table III.

The GT plant is equipped with a standard governor with 5% droop which its response is assumed to be linearly increased until 10 seconds [27]-[29]. This helps GT to deliver its maximum primary frequency response (PFR) [30]. The maximum loss-of-generation $\Delta P_{log,max}$ is simulated by tripping off the ST unit. Thus, the maximum PFR is 4% of the system's demand for 49.5 Hz as allowed steady-state frequency deviation [30], [31]. Apparent power of the GT unit, S_{gt}, is determined in such a way that its maximum rate-of-change-of-frequency (RoCoF) is limited to -0.5 Hz/s for the largest event [30]. Hence, this parameter must be greater than S_{min} percentage of system demand. It can be calculated as:

TABLE II
Power Flow of The Studied System (in % of the System Demand)

Unit	Load		GT plant			ST plant		Wind farm		STATCOM	
Case	*P*	*Q*	*S*	*P*	*Q*	*S*	*P*	*S*	*P*	*S*	*Q*
Case 1	100	10	95	66.4	6.8	5.9	5	40	28.8	4	3
Case 2	100	10	41.7	22.2	1.6	5.9	5	80	73.6	8	4.7
Case 3	100	10	96.7	67.7	6.4	5.9	5	50	27.5	5	3.7
Case 4	100	10	114	80	5.1	5.9	5	50	15	5	3.7

TABLE III
The Installed Capacities and Operating Points for Wind Turbines

WT number		1	2	3	4	5	6	7	8	9	10	Farm
Case 1	k_{ic}	4	4	4	4	4	4	4	4	4	4	40
	k_{op}	72	72	72	72	72	72	72	72	72	72	72
Case 2	k_{ic}	8	8	8	8	8	8	8	8	8	8	80
	k_{op}	92	92	92	92	92	92	92	92	92	92	92
Case 3	k_{ic}	0.91	1.82	2.73	3.64	4.55	5.45	6.36	7.27	8.18	9.09	50
	k_{op}	30	40	40	**55**	60	50	70	80	60	30	**55**
Case 4	k_{ic}	0.91	1.82	2.73	3.64	4.55	5.45	6.36	7.27	8.18	9.09	50
	k_{op}	**30**	0	0	0	0	50	55	55	55	0	**30**

This article has been accepted for publication in a future issue of this journal, but has not been fully edited. Content may change prior to final publication. Citation information: DOI 10.1109/TPWRS.2019.2939411, IEEE Transactions on Power Systems

$$S_{min} = \frac{f_{nom}}{M_{gt} RoCoF_{max}} \Delta P_{log,max} = \frac{50}{12 \times 0.5} \times 5 = 41.7\% \quad (55)$$

where, M_{gt} denotes mechanical time constant of GT. In addition, it is assumed that the active power of the GT, P_{gt}, is equal or lower than 0.7 of its rating capacity. Then, it yields:

$$S_{gt} = max\left(0.7^{-1} P_{gt}, S_{min}\right) \quad (56)$$

In this study, the extended WT type 4 IEC model is simulated as shown in Fig. 9 [32]. The *Wind Turbine* block models aerodynamics of the turbine using equations (1)-(8). The *MPPT* determines the optimal power. The *Drive Train* represents the mechanical parts of the turbine through a two-mass model [32]. The power controller illustrated in Fig. 10 modulates the active power of the WT plant. Here, the *Selector* block selects its top input; otherwise, other blocks will be ignored. Output of the *Flag_F* block will jump from zero to one when the GT frequency deviation is greater than F_db. It means Pref_IR and P_IR signals have values identical with optimal power P_mppt during normal system operation. The Tref_IRd and Pref_IRd denote the electrical torque and power references during the deceleration period of the WT's inertial response. The *Inertia emulator* contains (11)-(41) to implement the TLB methods. The speed recovery equations (50)-(51) are incorporated into the *IR_Pref* block. It deploys the turbine speed W and Flag_F as logical signals to determine the inertial power Pref_IR. The Rp_IRd and Rp_IRa are ramp rates during the deceleration and acceleration periods. The latter is set to the maximum value of the former one. The *Hold* block is considered to set the output at rising edge of Flag F.

In Fig. 8, the Wind Farm element models the gird side converters of 10 WT power plants with an equivalent converter. Fig. 11 shows how reference value of its direct axis current is calculated based on the reference power of the WT plants and voltage amplitude of the wind farm terminal.

B. Frequency Response with Medium Wind Penetration

In the first case study, the installed capacity of the wind farm is 40% and all of the 10 WTs operate with $k_{op} = 72\%$. In this condition, the kinetic energy released from rotor of WTs has maximum value for the conventional TLB scheme (See Fig. 4.a). The system frequency response to ST's tripping is illustrated in Fig. 12. To get better insight into the system operation, the power traces are represented in percentage of the system demand. The results are shown for three scenarios. The inertial response of the WTs is deactivated in the *No Inertia* scenario. The WTs inertial response is governed by the modified conventional and the proposed TLB methods in the *Conventional* and *Proposed* scenarios, respectively. As previously shown in Fig. 4 and Fig. 5, the released kinetic

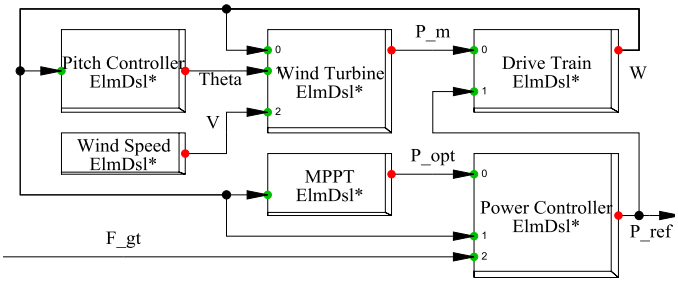

Fig. 9. Block diagram of the proposed WT Power Plant in PowerFactory.

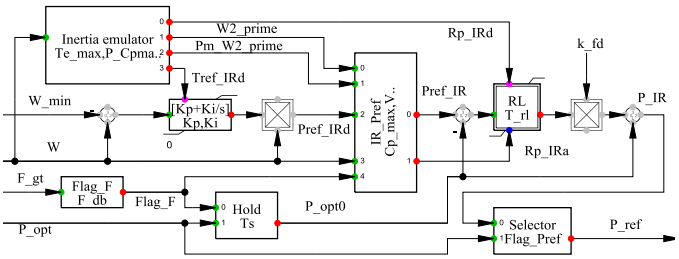

Fig. 10. Block diagram of the WT Power Controller in PowerFactory.

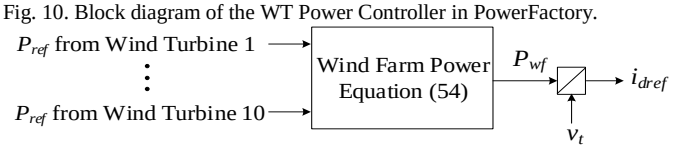

Fig. 11. Schematic for the wind farm's power calculation process.

energy and torque ramp rate quantities have the maximum and minimum values, when N is 3 in the proposed method. It can be deduced that the proposed TLB technique is customized based on the wind turbines' power. It can be seen from Fig. 12 that although the wind farm generates more inertial power using the conventional scheme, the GT's frequency nadir is deteriorated. However, it improves the RoCoF. This is due to the fact that the maximum increment of the farm's electrical power is about two times of the disturbance size. On the other hand, the results indicate that the proposed scheme is able to improve the frequency nadir, while maintaining a positive effect to reduce RoCoF.

To understand the *IR_Pref* block in Fig. 10, its logical flags are shown in Fig. 13. Some of these traces are scaled. The frequency dead-band required for activation of the inertia emulator is assumed to be 0.1 Hz. When the GT frequency deviation reaches 0.1 Hz, then the Flag F jumps to 1 and

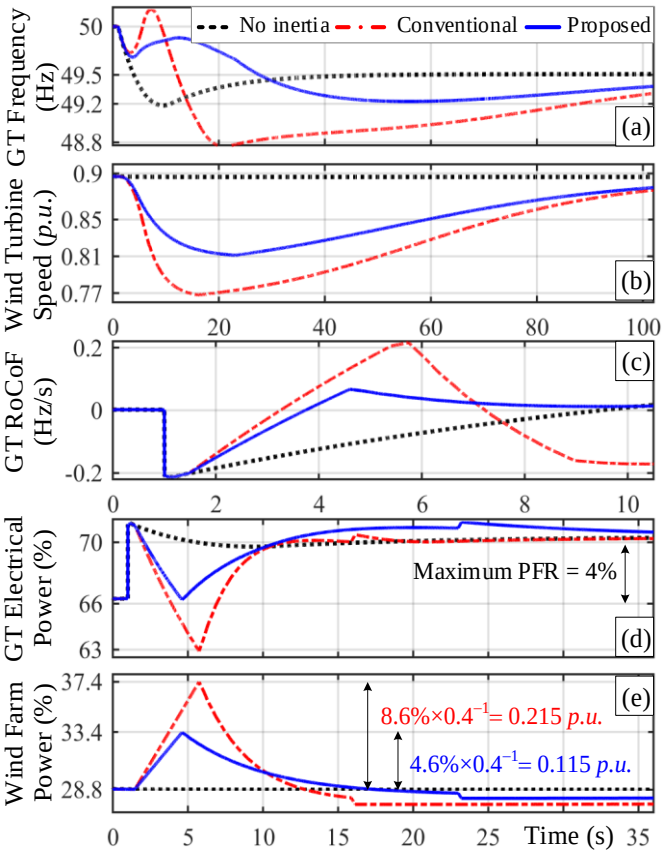

Fig. 12. Simulation results of case study 1 ($k_{ic} = 40\%$ and $k_{op} = 72\%$).

This article has been accepted for publication in a future issue of this journal, but has not been fully edited. Content may change prior to final publication. Citation information: DOI 10.1109/TPWRS.2019.2939411, IEEE Transactions on Power Systems

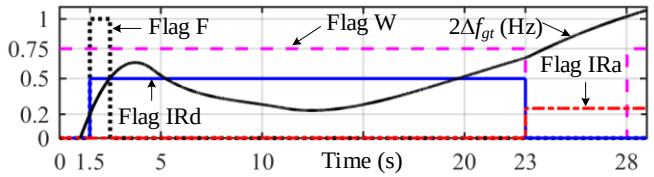

Fig. 13. Case study 1: the logical flags for the proposed TLB scheme.

remains constant up to 1 second. The Flag W is set to 1 if the WT speed is greater than 100.1% of ω_2', otherwise, it is set to 0. To prevent redundant switching at the beginning of the WT's speed recovery, Flag W remains constant up to 5 seconds when it drops to 0. If the Flag W is 1, the Flag IRd varies from 0 to 1 at rising edge of the Flag F. This flag will reset to 0 when the Flag W is 0, otherwise, it holds its old value. The Flag IRa changes from 0 to 1 at falling edge of the Flag IRd, otherwise, it remains at its old value.

C. Frequency Response with High Wind Penetration

In the second case, the installed capacity of the farm is increased from 40% to 80%. In addition, the WTs operate at 92% of their capacities where the turbines release identical kinetic energy under TLB schemes. It is notable that the higher wind generation causes system inertia reduction. Therefore, Gt's rating is limited to S_{min} to restrict its RoCoF to -0.5 Hz/s. The frequency response of the studied system is shown in Fig. 14. It is observed that the GT's frequency nadir is significantly decreased when the conventional and proposed

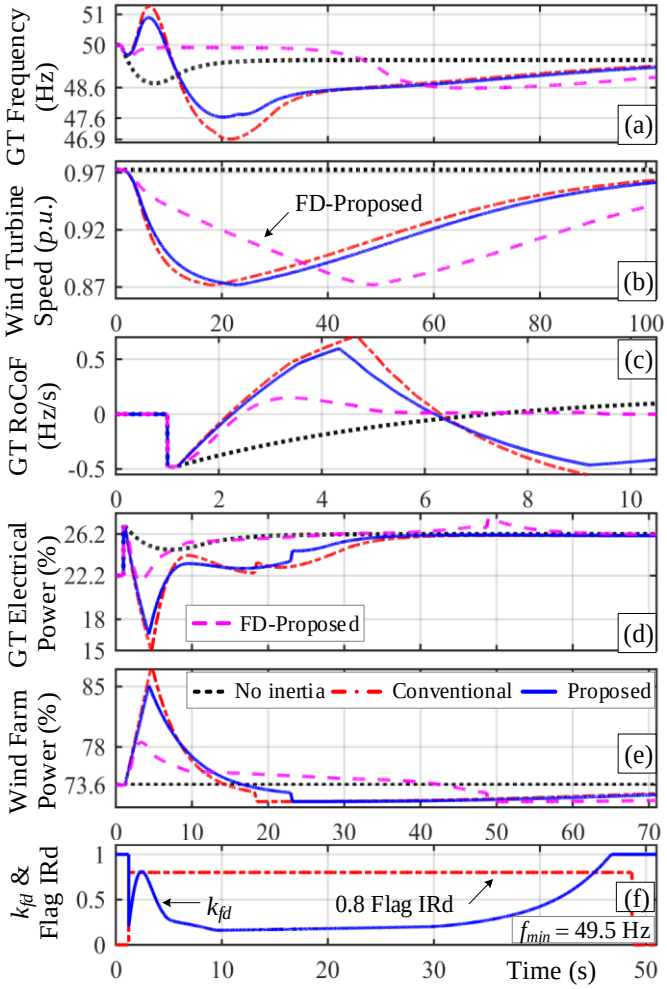

Fig. 14. Simulation results of case study 2 (k_{ic} = 80% and k_{op} = 92%).

TLB methods are used. By comparing Figs. 14.d and 14.e, it can be concluded that the wind farm response is not coordinated with that of the GT in these scenarios. To solve this problem, a frequency-dependent coefficient is defined as:

$$k_{fd} = \begin{cases} min\left[\left(f_{gt} - f_{min}\right)\left(f_{min} - f_{nom}\right)^{-1}, 1\right] & \text{Flag IRd} > 0 \\ 1 & \text{Otherwise} \end{cases} \quad (57)$$

where, f_{nom} and f_{gt} are nominal and measured frequencies of the GT in Hz. In fact, k_{fd} is linearly increased from zero to one when the GT frequency decreases from f_{nom} to f_{min}. As shown in Fig. 10, the inertial response of the WT can be modified by multiplying it by k_{fd}. The *FD-Proposed* scenario shown in Fig. 14 corresponds to the modified scheme under f_{min} = 49.5 Hz. This method considerably improves system frequency especially its nadir by coordinating the GT's and WT's responses. In this scenario, the delayed WT speed recovery allows the system operator to release primary reserves and mitigate the second frequency dip at t = 50 s.

D. Estimation of the Wind Farm's Inertial Response

In real world, the wind farms are located in different geographical locations with different wind speeds. Moreover, turbines with various ratings and dissimilar operating points may construct a farm. For example, the total installed capacity of the wind farm is 50% in cases 3 and 4 while it is not similar for each individual wind turbines. Also, the turbines' operating points are totally different. Let's suppose that only the farm's generated power is known. An interesting question that arises is how the wind farm's inertial response can be estimated. To this end, the averaging technique is proposed. In other words, the estimated power has similar shape with those wind turbines which have identical operating point with wind farm's averaged operating point. With reference to Table III, these target turbines are WT 4 and WT 1 in Case 3 and Case 4, respectively. Their estimated inertial powers are compared with their true values in Figs. 15 and 16, respectively. It can be seen that the estimation error is considerable if the modified conventional TLB scheme is deployed, especially when operating points of the individual turbines differs significantly with respect to averaged operating point of the farm, as shown in case 4. On the other hand, the linear characteristics of the proposed TLB strategy results in negligible estimation errors.

VI. Conclusions

In this paper, the conventional torque limit-based (TLB) method is firstly modified considering a definite ramp rate for inertial power of wind turbines (WT). It is revealed that the kinetic energy released by the WT's rotor is maximized at medium WT's rotor speed due to the non-linear relationship between the conventional TLB scheme's features and the WT operating point. Secondly, a linear TLB strategy is proposed by customizing its key parameters to obtain a linear relation between its characteristics and the WT's operating point. In particular, the amount of the released kinetic energy and power ramp rate can be chosen in proportion of the pre-event values of power, rotor speed and or reserved rotor kinetic energy of the WT. It is shown that the suggested TLB method put lower stress on the mechanical parts of the turbine, especially at low rotor speeds, in comparison with the conventional one. However, the latter one can provide more

This article has been accepted for publication in a future issue of this journal, but has not been fully edited. Content may change prior to final publication. Citation information: DOI 10.1109/TPWRS.2019.2939411, IEEE Transactions on Power Systems

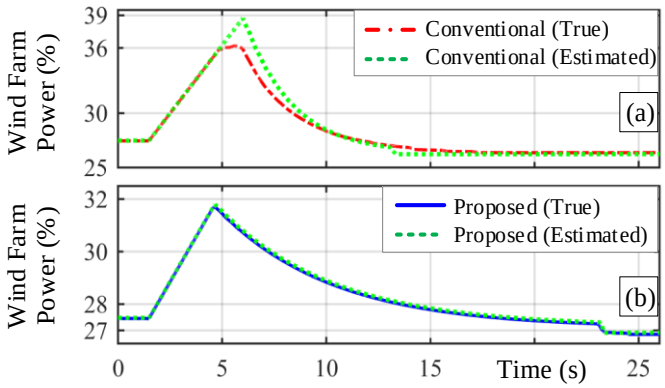

Fig. 15. Simulation results of case study 3 ($k_{ic} = 50\%$ and $k_{op} = 55\%$).

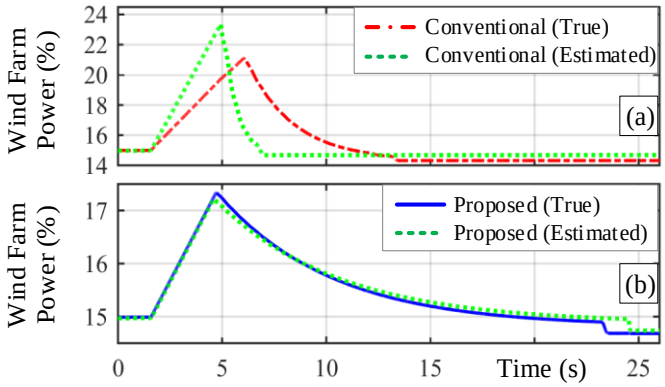

Fig. 16. Simulation results of case study 4 ($k_{ic} = 50\%$ and $k_{op} = 30\%$).

inertial energy. The effectiveness of the discussed TLB methods is investigated through a power system under different wind penetration levels. The results illustrate that the suggested inertia emulation strategy ensures more secure system operation. However, while the wind penetration is high, the incoordination between the WTs inertial response and governor response of the fossil-fueled unit deteriorates the frequency nadir for both TLB schemes. In order to tackle this challenge, it is suggested that the WT's inertial power should be multiplied by a frequency-dependent gain. The study also shows that when the parameters of the proposed method is designed based on the WT's power, the inertial response of a wind farm can be exactly estimated only by using total generation of the farm, regardless of its turbines installed capacities and operating points. Finally, a new approach is also projected to estimate the inertial response of the WT during the deceleration period using an analytical closed-form function which facilitates large scale system studies.

REFERENCES

[1]B. Kroposki, B. Johnson, Y. Zhang, V. Gevorgian, P. Denholm, B. M. Hodge, and B. Hannegan, "Achieving a 20% renewable grid: Operating electric power systems with extremely high levels of variable renewable energy," *IEEE Power Energy Mag.*, vol. 12, no. 2, pp. 24-73, Mar. 2017.

[2]R. Azizipanah-Abarghooee, M. Malekpour, Y. Feng, and V. Terzija, "Modeling DFIG-based system frequency response for frequency trajectory sensitivity analysis," *Int. Trans. Electr. Energy Syst.*, vol. 29, no. 4, pp. 1-17, Apr. 2019.

[3]J. Ekanayake and N. Jenkins, "Comparison of the response of doubly fed and fixed-speed induction generator wind turbines to changes in network frequency," *IEEE Trans. Energy Convers.*, vol. 19, no. 4, pp. 800-802, Dec. 2004.

[4]A. Mullane and M. O'Malley, "The inertial response of induction-machine-based wind turbines," *IEEE Trans. Power Syst.*, vol. 20, no. 3, pp. 1096-1203, Aug. 2005.

[5]G. Ramtharan, J. B. Ekanayake and N. Jenkins, "Frequency support from doubly fed induction generator wind turbines," *IET Renew. Power Gener.*, vol. 1, no. 1, pp. 3-9, Mar. 2007.

[6]M. Kayikci and J. V. Milanovic, "Dynamic contribution of DFIG-based wind plants to system frequency disturbances," *IEEE Trans. Power Syst.*, vol. 24, no. 2, pp. 822-867, May 2009.

[7]J. Lee, G. Jang, E. Muljadi, F. Blaabjerg, Z. Chen and Y. Cheol Kang, "Stable short-term frequency support using adaptive gains for a DFIG-based wind power plant," *IEEE Trans. Energy Convers.*, vol. 31, no. 3, pp. 1068-1079, Sep. 2016.

[8]Y. Wu, W. Yang, Y. Hu and P. Q. Dzung, "Frequency regulation at a wind farm using time-varying inertia and droop controls," *IEEE Trans. Ind. App.*, vol. 55, no. 1, pp. 213-224, Jan.-Feb. 2019.

[9]A. Bonfiglio, M. Invernizzi, A. Labella and R. Procopio, "Design and implementation of a variable synthetic inertia controller for wind turbine generators," *IEEE Trans. Power Syst.*, vol. 34, no. 1, pp. 754-764, Jan. 2019.

[10] L. Xiong, P. Li, F. Wu and J. Wang, "Stability enhancement of power systems with high dfig-wind turbine penetration via virtual inertia planning," *IEEE Trans. Power Syst.*, vol. 34, no. 2, pp. 1352-1361, Mar. 2019.

[11] M. Kang, K. Kim, E. Muljadi, J. W. Park and Y. C. Kang, "Frequency control support of a doubly-fed induction generator based on the torque limit," *IEEE Trans. Power Syst.*, vol. 31, no. 6, pp. 4205-4213, Nov. 2016.

[12] D. Yang, J. Kim, Y. C. Kang, E. Muljadi, N. Zhang, J. Hong, S. H. Song, and T. Zheng, "Temporary frequency support of a dfig for high wind power penetration," *IEEE Trans. Power Syst.*, vol. 33, no. 3, pp. 3428-3437, May 2018.

[13] J. F. Conroy and R. Watson, "Frequency response capability of full converter wind turbine generators in comparison to conventional generation," *IEEE Trans. Power Syst.*, vol. 23, no. 2, pp. 245-656, May 2008.

[14] M. Garmroodi, G. Verbič and D. J. Hill, "Frequency support from wind turbine generators with a time-variable droop characteristic," *IEEE Trans. Sustain. Energy*, vol. 9, no. 2, pp. 676-684, Apr. 2018.

[15] K. Liu, Y. Qu, H. M. Kim and H. Song, "Avoiding frequency second dip in power unreserved control during wind power rotational speed recovery," *IEEE Trans. Power Syst.*, vol. 33, no. 3, pp. 3097-326, May 2018.

[16] M. Altin, A. D. Hansen, T. K. Barlas, K. Das and J. N. Sakamuri, "Optimization of short-term overproduction response of variable speed wind turbines," *IEEE Trans. Sustain. Energy*, vol. 9, no. 4, pp. 1732-1739, Oct. 2018.

[17] S. Wang and K. Tomsovic, "A novel active power control framework for wind turbine generators to improve frequency response," *IEEE Trans. Power Syst.*, vol. 33, no. 6, pp. 6579-6589, Nov. 2018.

[18] Y. Tan, L. Meegahapola and K. M. Muttaqi, "A suboptimal power-point-tracking-based primary frequency response strategy for DFIGs in hybrid remote area power supply systems," *IEEE Trans. Energy Convers.*, vol. 31, no. 1, pp. 93-25, Mar. 2016.

[19] M. Fischer, S. Engelken, N. Mihov and A. Mendonca, "Operational experiences with inertial response provided by type 4 wind turbines," *IET Renew. Power Gener.*, vol. 2, no. 1, pp. 17-24, Jan. 2016.

[20] S. Engelken, A. Mendonca and M. Fischer, "Inertial response with improved variable recovery behaviour provided by type 4 WTs," *IET Renew. Power Gener.*, vol. 9, no. 3, pp. 195-201, Jan. 2017.

[21] T. Burton, N. Jenkins, D. Sharpe, and E. Bossanyi. *Wind energy handbook*. John Wiley & Sons, 2011.

[22] S. Heier, *Grid integration of wind energy conversion systems*, 2nd Edition, Wiley, April 2006.

[23] J. Fortmann, *Modeling of Wind Turbines with Doubly Fed Generator System*. Springer, 2014.

[24] H. Ye, W. Pei and Z. Qi, "Analytical modeling of inertial and droop responses from a wind farm for short-term frequency regulation in power systems," *IEEE Trans. Power Syst.*, vol. 31, no. 5, pp. 3414-3423, Sep. 2016.

[25] R. Azizipanah-Abarghooee, M. Malekpour, M. Zare, and V. Terzija. "A new inertia emulator and fuzzy-based LFC to support inertial and governor responses using Jaya algorithm," *IEEE Power Energy Soc. Gen. Meet. (PESGM)*, pp. 1-5, Jul. 2016.

[26] C. Concordia and S. Ihara, "Load representation in power system stability studies," *IEEE Trans. Power App. Syst.*, vol. PAS-101, no. 4, pp. 969-977, Apr. 1982.

[27] P. Kundur, N. J. Balu, and M. G. Lauby, *Power System Stability and Control*. New York: McGraw-Hill, 1994.

[28] R. Azizipanah-Abarghooee, M. Malekpour, M. Paolone, and V. Terzija, "A new approach to the online estimation of the loss of generation size in power systems," *IEEE Trans. Power Syst.*, vol. 34, no. 3, pp. 2103-2113, May 2019.
[29] R. Azizipanah-Abarghooee, M. Malekpour, M. S. Ayaz, M. Karimi, and V. Terziia, Small signal based frequency response analysis for power systems, *IEEE PES Innov. Smart Grid Tech. Conf. Europe (ISGT-Europe)*, pp. 1-6, Oct. 2018.
[30] F. Teng, V. Trovato, and G. Strbac, "Stochastic scheduling with inertia-dependent fast frequency response requirements," *IEEE Trans. Power Syst.*, vol. 31, no. 2, pp. 1557-1566, Mar. 2016.
[31] M. Malekpour, R. Azizipanah-Abarghooee, F. Teng, G. Strbac, and V. Terzija, "Fast frequency response from smart induction motor variable speed drives," *IEEE Trans. Power Syst.*, To be published, 2019.
[32] A. D. Hansen and I. D. Margaris, "Type IV wind turbine model," DTU Wind Energy, Tech. Rep., 2014.

Rasoul Azizipanah-Abarghooee (S'15-M'18-SM'19) received the BEng degree from Isfahan University of Technology, Iran, in 2010, and the MEng and PhD degrees with highest honors from Shiraz University of Technology, Iran, in 2012 and 2016, respectively, all in power electrical engineering. He received his second PhD degree with honor from University of Manchester, U.K. in 2018.

He is the Postdoctoral Research Associate in the Department of Electrical and Electronic Engineering, University of Manchester, U.K. leading EFCC and Supergen Energy Network Hub (ICT & Data) projects. The earlier one became a candidate for Scottish Green Energy Awards and got British Renewable Energy Awards in 2018.

Since September 2017, he has been also collaborating as a visiting scholar with the Electricity System Operator at National Grid; Distributed Electrical Systems Laboratory (DESL) at the Swiss Federal Institute of Technology of Lausanne (EPFL); Control and Power System Group at Imperial College London; and Department of Energy Technology at Aalborg University. He was a keynote speaker at IET and EFCC events in Glasgow and Cheltenham, UK in Feb. 2018 and Mar. 2018, respectively. His research interests include application of wide-area monitoring and control systems; multi-vector energy networks; application of power electronics; power system stability, dynamic, market and operation; practical forecasting and probabilistic programming.

Dr. Azizipanah-Abarghooee serves as an Associate Editor of International Journal of Electrical Power and Energy Systems. He was a recipient of several fellowship awards from Iran National Elites Foundation.

He is nominated in 2018 by Thomson Reuters to be the world's top 1% researchers in Engineering.

Mostafa Malekpour (S'18) received the B.Sc. degree from Isfahan University of Technology, Isfahan, Iran, in 2010, and the M.Sc. degree from Shiraz University of Technology, Shiraz, Iran, in 2013, all in power electrical engineering. He is currently pursuing the Ph.D. degree in electrical engineering at the University of Isfahan, Isfahan, Iran. Since January 2017, he has also been collaborating with the Department of Electrical and Electronic Engineering, University of Manchester, Manchester, U.K. In 2018 and 2019, he received the Best Reviewer Award in recognition of his remarkable contributions in International Journal of Electrical Power and Energy Systems. His research interests include power system dynamics and grid integration of renewable energy sources.

Tomislav Dragičević (S'09-M'13-SM'17) received the M.Sc. and the industrial Ph.D. degrees in Electrical Engineering from the Faculty of Electrical Engineering, Zagreb, Croatia, in 2009 and 2013, respectively. From 2013 until 2016 he has been a Postdoctoral research associate at Aalborg University, Denmark. From March 2016 he is an Associate Professor at Aalborg University, Denmark where he leads an Advanced Control Lab.

He made a guest professor stay at Nottingham University, UK during spring/summer of 2018. His principal field of interest is design and control of microgrids, and application of advanced modeling and control concepts to power electronic systems. He has authored and co-authored more than 170 technical papers (more than 70 of them are published in international journals, mostly IEEE Transactions) in his domain of interest, 8 book chapters and a book in the field.

He serves as Associate Editor in the IEEE TRANSACTIONS ON INDUSTRIAL ELECTRONICS, in IEEE Emerging and Selected Topics in Power Electronics and in IEEE Industrial Electronics Magazine. Dr. Dragičević is a recipient of the Končar prize for the best industrial PhD thesis in Croatia, and a Robert Mayer Energy Conservation award.

Frede Blaabjerg (S'86–M'88–SM'97–F'03) was with ABB-Scandia, Randers, Denmark, from 1987 to 1988. From 1988 to 1992, he got the PhD degree in Electrical Engineering at Aalborg University in 1995. He became an Assistant Professor in 1992, an Associate Professor in 1996, and a Full Professor of power electronics and drives in 1998. From 2017 he became a Villum Investigator. He is honoris causa at University Politehnica Timisoara (UPT), Romania and Tallinn Technical University (TTU) in Estonia.

His current research interests include power electronics and its applications such as in wind turbines, PV systems, reliability, harmonics and adjustable speed drives. He has published more than 600 journal papers in the fields of power electronics and its applications. He is the co-author of four monographs and editor of ten books in power electronics and its applications.

He has received 31 IEEE Prize Paper Awards, the IEEE PELS Distinguished Service Award in 2009, the EPE-PEMC Council Award in 2010, the IEEE William E. Newell Power Electronics Award 2014, the Villum Kann Rasmussen Research Award 2014 and the Global Energy Prize in 2019. He was the Editor-in-Chief of the IEEE TRANSACTIONS ON POWER ELECTRONICS from 2006 to 2012. He has been Distinguished Lecturer for the IEEE Power Electronics Society from 2005 to 2007 and for the IEEE Industry Applications Society from 2010 to 2011 as well as 2017 to 2018. In 2019-2020 he serves a President of IEEE Power Electronics Society. He is Vice-President of the Danish Academy of Technical Sciences too.

He is nominated in 2014-2018 by Thomson Reuters to be between the most 250 cited researchers in Engineering in the world.

Vladimir Terzija (M'95–SM'00-F'16) was born in Donji Baraci (former Yugoslavia). He received the Dipl-Ing., M.Sc., and Ph.D. degrees in electrical engineering from the University of Belgrade, Belgrade, Serbia, in 1988, 1993, and 1997, respectively.

He is the Engineering and Physical Science Research Council (EPSRC) Chair Professor in Power System Engineering with the Department of Electrical and Electronic Engineering, The University of Manchester, Manchester, U.K., where he has been since 2006. From 1997 to 1999, he was an Assistant Professor at the University of Belgrade, Belgrade, Serbia. From 2000 to 2006, he was a senior specialist for switchgear and distribution automation with ABB, Ratingen, Germany. His current research interests include smart grid applications; wide-area monitoring, protection, and control; multi-energy systems; switchgear and transient processes; ICT, data analytics and digital signal processing applications in power systems.

Prof. Terzija is Editor in Chief of the International Journal of Electrical Power and Energy Systems, Alexander von Humboldt Fellow, as well as a DAAD and Taishan Scholar. He is the recipient of the Qilu Friendship Award, China (2018). Since 2018, he is the National Thousand Talents Distinguished Professor at Shandong University, China.